An Introduction to Plasmonics

S Dutta Gupta
School of Physics, University of Hyderabad
Hyderabad 500046, INDIA
email: sdghyderabad@gmail.com
web: https://www.tifrh.res.in/ sdg/index.html

November 11, 2021

Contents

Chapter 1

Introduction

Plasmonics opens up the gateway to the sub-wavelength world by its inherent ability to beat the Rayleigh limit. What is truly amazing is the fact that most of the related effects can be understood with an undergraduate background of classical optics, and all of it was around for so many years. Indeed the past two decades have been an eyeopener to novel effects arising from classical Maxwellian optics. Superlensing and super resolution, invisibility cloaks, extraordinary transmission are just a few examples. One now understands a large variety of effects under the banner of plasmonics with potential applications ranging from enhanced photovoltaics to imaging, surface enhanced spectroscopy to the precision spectroscopy of single molecules. In fact, there are many more unexplored areas.

I have a very humble goal in these lectures: to lay open the basic entity, namely the surface plasmons (SP's). Perhaps the best possible source to learn about surface plasmons even today is the monograph of Raether[1]. I will try to show how the SP, being the closest kin of guided modes of an equivalent dielectric structures, is so very different from them. I won't discuss the free electron model or the bulk plasmons of noble metals. One can find a nice description in the monograph by Maier [3]. Nor would I try to highlight all the important applications (see part II of [3]). Nevertheless, I will try to highlight the physics which opens up the possibilities for all such applications.

In standard textbooks or monographs the surface plasmons and related phenomena are introduced starting from a single metal-dielectric interface. One then moves on to two or more interfaces yielding coupled plasmons and gap plasmons. This approach is good for beginners but lacks the bird's eye view of many related phenomena. In my teaching experience I have encountered students who miss out on the similarities and differences between the guided and the surface modes. In these notes I have tried to adopt a different approach, namely, move from general to specific situations. We start with a multilayered metal-dielectric stratified medium, in order to have a general framework encompassing a wide spectrum of effects. We show how the characteristics of the modes can be calculated through the poles of the reflection/transmission coefficients, which is the same as solving the dispersion relation. We specialize to a simpler case study, where we look at the modes of a general symmetric layered medium, which simplifies the equations and at the outset distinguishes the symmetric and antisymmetric modes. We then consider various limiting cases yielding the well known results for waveguide modes, surface plasmons (both long and short range), and the gap plasmon modes. While most of this is a blackboard excercise, I have borrowed few results from my earlier papers involving not-so-simple numerical calculations (multi-branch dispersion curves). The latter will be presented in the notes and in order to maintain a smooth flow, I will try not to switch to slides.

The structure of these notes are as follows. In Chapter 2, we start with the derivation of the amplitude reflection and transmission coefficients [4, 5], we define the modes of the structure through the poles of these cofficients. We take a particular case of a symmetric structure [6], which enables us to arrive at the dispersion relations of the symmetric and the antisymmetric modes. By taking suitable limits we show that these dispersion relations are identical to the standard forms. We solve the dispersion relations for simple cases of planar waveguides and coupled plasmons. We show that while waveguide dispersion can be calculated easily by "cheating", the same is not possible for the coupled plasmons. We present a simple matlab code highlighting the complexities of the root finder and few other sources of problems related to causality. In order to highlight the near field or the sub-wavelength capabilities of plasmonics we then consider a gap plasmon (GP) guide where a sub-wavelength dielectric layer is enclosed in between two semi-infinite/finite metal layers. The fundamental plasmonic mode can propagate in this guide while any TE mode is prohibited by the Rayleigh criterion. In this context we demonstrate an avoided crossing phenomenon, which is often encountered in optical and solid state systems. Chapter 2 gives few more details about the surface plasmons and coupled surface plasmons, concentrating mainly on how to excite them. Of course, methods discussed here are not exhaustive, but they serve the purpose of highlighting the role of momentum matching. A brief comparison is made with the quasi phase matching in nonlinear optics. Chapter 3 deals with a wider spectum of effects which are also applicable to plasmonic structures. The goal here was to open up the possibilities of the plasmonic structures to explore effects hitherto known in atomic samples and quantum well/barrier systems.

Chapter 2

Reflection and Transmission through Layered Media and Eigenmodes

2.1 Characteristic Matrices

Consider the j-th slab of the stratified medium shown in Fig.2.1 with dielectric function ε_j occupying the space between planes $z = z_j$ and $z = z_{j+1}$ (let $d_j = z_{j+1} - z_j$ be the width). Let $y = 0$ be the plane of incidence. Because of our intention of exploring the plasmonic phenomena in these notes, we restrict our attention only to the TM-modes (with non-vanishing components H_y, E_x *and* E_z). Since noble metals are known to possess strong dispersion, we shall be incorporating available experimental data via suitable interpolation scheme like spline interpolation [7, 8]. All the media are also assumed to be nonmagnetic. For TM-polarized light the only non-vanishing magnetic field component is H_y for the aforementioned slab can be written as

$$H_{jy} = A_{j+}e^{ik_{jz}(z-z_j)} + A_{j-}e^{-ik_{jz}(z-z_j)}, j = 1 \cdots N, \tag{2.1}$$

while the expression for the corresponding tangential component of the electric field E_{jx} is given by

$$E_{jx} = p_{jz}(A_{j+}e^{ik_{jz}(z-z_j)} - A_{j-}e^{-ik_{jz}(z-z_j)}). \tag{2.2}$$

In Eqs.(2.1) and (2.2), $A_{j\pm}$ are the forward and backward wave amplitudes, while k_{jz} and p_{jz} are expressed through the x-component of the propagation constant k_x as

$$k_{jz} = \sqrt{k_0^2\varepsilon_j - k_x^2}, p_{jz} = \frac{k_{jz}}{k_0\varepsilon_j}, k_0 = \frac{\omega}{c}. \tag{2.3}$$

In Eq.(3) one has to ensure that the imaginary part of the z-component of the wave vector is positive. Writing Eqs. (1) and (2) on the left and right faces of the j-th layer, one can relate the corresponding tangential field components by the matrix relation

$$\begin{pmatrix} H_y \\ E_x \end{pmatrix}_j = M_j \begin{pmatrix} H_y \\ E_x \end{pmatrix}_{j+1}, \tag{2.4}$$

where the subscript j refers to $z = z_j$ and the characteristic matrix M_j is given by [4]

$$M_j = \begin{pmatrix} \cos(k_{jz}d_j) & -(i/p_{jz})\sin(k_{jz}d_j) \\ -ip_{jz}\sin(k_{jz}d_j) & \cos(k_{jz}d_j) \end{pmatrix} \tag{2.5}$$

For a layered medium with N layers as in Fig.1, the total characteristic matrix is given by

$$M_{total} = M_1 M_2 .... M_N. \tag{2.6}$$

Later the characteristics matrix was generalized to Kerr nonlinear stratified media and applied to explore various nonlinear optical effects and photon localization in nonlinear systems [5].

2.2 Amplitude Reflection and Transmission Coefficients and Dispersion Relation

In this section we present the results for the reflection and transmission features of a layered structure (see Fig.2.1). Let the structure be illuminated by a plane monochromatic wave at an angle θ_i. The amplitude reflection (r) and transmission (t) coefficients of such a structure are given by [4, 5]:

$$\begin{aligned} r &= \frac{(m_{11} + m_{12}p_f)p_i - (m_{21} + m_{22}p_f)}{(m_{11} + m_{12}p_f)p_i + (m_{21} + m_{22}p_f)} \\ t &= \frac{2p_i}{(m_{11} + m_{12}p_f)p_i + (m_{21} + m_{22}p_f)} \end{aligned} \tag{2.7}$$

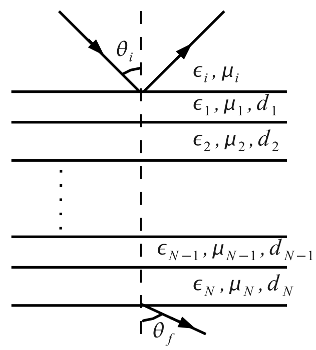

Figure 2.1: Schematic of a layered structure.

where m_{ij} $(i, j = 1, 2)$ are the elements of the total characteristic matrix of the structure (see Eq.(2.6)) and we have suppressed z from the subscripts of p. The intensity reflection (R) and transmission (T) of the structure are given by $R = |r|^2$ and $T = |t|^2$ (for identical media of incidence and emergence).

Note that a common denominator figures in the expressions of both the reflection and transmission coefficients (Eq.(2.7)). The zeroes of the denominator bear the information about the characteristic frequencies (eigenfrequencies) of the system. Physically this corresponds to the situation when with no input certain specific disturbances can be maintained in the system. Such specific disturbances with well defined spatial profiles are referred to as the modes of the structure. The corresponding equation (also known as the dispersion relation) can be written as [5, 9]

$$D = (m_{11} + m_{12}p_f)p_i + (m_{21} + m_{22}p_f) = 0 \ , \tag{2.8}$$

The dispersion relation (2.8) can be solved in general for complex roots, which carries all the information about the modes and their associated decay rates. In fact, the real part of the roots gives the locations of the modes, while the imaginary part corresponds to the width of these resonances. Due to the transcendental nature of Eq. (2.8), in general, it cannot be solved analytically. One has to revert to a graphical or numerical scheme to obtain the distinct branches for the modes.

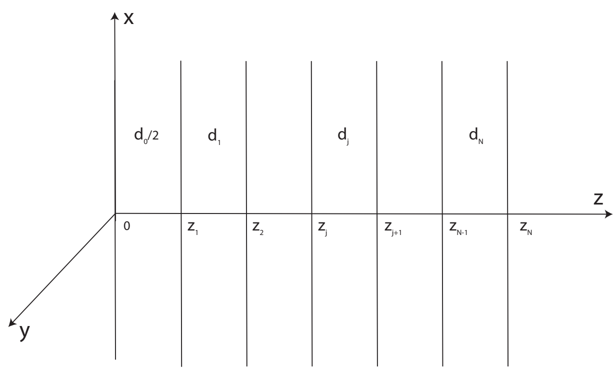

Figure 2.2: Schematic view of the symmetric layered medium, where only the right half is shown.

2.3 Case Study: A symmetric $(2N+1)$-layer structure

Consider the TM-modes (with non-vanishing components $H_y, E_x\ and\ E_z$) for the symmetric system shown in Fig. 2.2, comprising of $2N+1$ layers with any j-th layer characterized by a dielectric function $\varepsilon_j(\omega)$ and width d_j. The middle layer is assumed to have a width d_0 and dielectric function ε_0 (symbol not to be confused with the vacuum dielectric permittivity). The bounding media are assumed to be air. Like before we restrict our attention only to the TM polarized waves. Keeping in view the symmetry of the structure about the plane $z=0$, we write the magnetic and electric field components in the central layer as

$$\begin{aligned} H_{0y} &= A_0(e^{ik_{0z}z} \pm e^{-ik_{0z}z}), & (2.9) \\ E_{0x} &= p_{0z}A_0(e^{ik_{0z}z} \mp e^{-ik_{0z}z}), & (2.10) \end{aligned}$$

where $k_{0z} = \sqrt{k_0^2\varepsilon - k_x^2}$ and $p_{0z} = \frac{k_{0z}}{k_0\varepsilon}$. Hereafter the upper (lower) sign in Eqs.(2.9) and (2.10) will refer to the symmetric (antisymmetric) magnetic modes. Note that symmetry is being judged by the symmetry of the magnetic field distribution across the layers. Making use of the characteristic matrices one can then relate the tangential field components at the centre, i.e., at z=0 and at $z = z_N$, which, in terms of amplitudes yields the following relation

$$\begin{pmatrix} 1 & \pm 1 \\ p_{0z} & \mp p_{0z} \end{pmatrix} \begin{pmatrix} A_0 \\ A_0 \end{pmatrix} = M_T \begin{pmatrix} 1 \\ p_{tz} \end{pmatrix} A_t. \qquad (2.11)$$

In Eq.(2.11) the subscript t refers to the corresponding quantities in the embedding medium and M_T is given by

$$M_T = M_0(d_0/2)M_1(d_1)\cdots M_j(d_j)\cdots M_N(d_N). \tag{2.12}$$

Referring to the different signs in Eq.(2.11) and demanding the nontriviality of the constant amplitudes, one obtains the dispersion relation for the symmetric and the antisymmetric modes. For the symmetric mode one has

$$\begin{aligned} m_{21} + m_{22}p_{tz} &= 0, & (2.13)\\ (m_{11} + m_{12}p_{tz})A_t &= 2A_0, & (2.14) \end{aligned}$$

while for the antisymmetric mode one obtains

$$\begin{aligned} m_{11} + m_{12}p_{tz} &= 0, & (2.15)\\ (m_{21} + m_{22}p_{tz})A_t &= 2p_{0z}A_0. & (2.16) \end{aligned}$$

It is clear that Eqs.(2.13) and (2.15) give the corresponding dispersion relations while (2.14) and (2.16) define the amplitudes for the mode functions.

2.4 Typical example: Modes of a Symmetric Waveguide

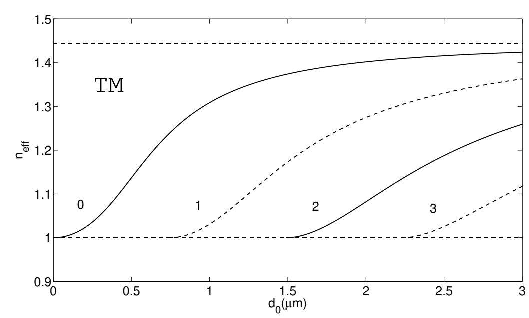

Figure 2.3: Transverse magnetic modes of a symmetric dielectric wave guide for parameters $\lambda = 1.55\mu m$, $\varepsilon_d = 2.085$ and $\varepsilon_t = 1.0$.

As an example, we first consider the case of a symmetric planar waveguide, whereby a slab of sielectric constant ε_d and width d_0 is embedded in a dielectric medium with dielectric constant ε_t (see Fig. 2.2 with $d_j = 0,\ j = 1 - N$).

For guided modes waves need to be evanescent outside the film. We thus rewrite k_{tz} as

$$k_{tz} = i\sqrt{k_x^2 - k_0^2\varepsilon_t} = i\bar{k}_{tz}. \tag{2.17}$$

Equations (2.13) and (2.15) can then be reduced to the well known dispersion relations for the symmetric and antisymmetric transverse magnetic modes of a planar guide

$$\varepsilon_d\bar{k}_{tz} - \varepsilon_t k_{0z}\tan(k_{0z}d_0/2) = 0, \tag{2.18}$$

$$\varepsilon_d\bar{k}_{tz} + \varepsilon_t k_{0z}\cot(k_{0z}d_0/2) = 0. \tag{2.19}$$

2.5 Relevant example: Surface Plasmons and Coupled Surface Plasmons

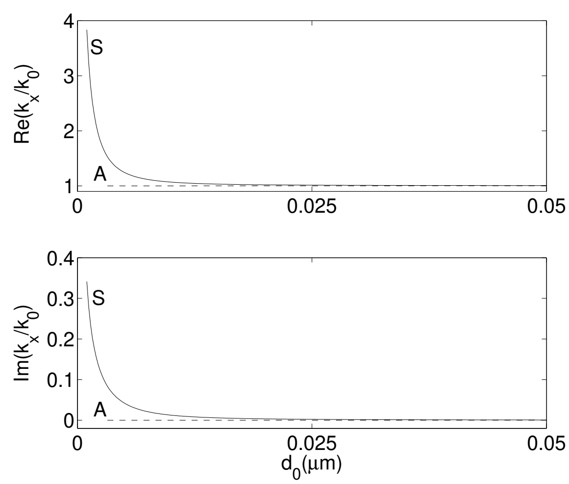

Figure 2.4: Real and imaginary parts of the normalized propagation constant k_x/k_0 for the coupled modes. The parameters are as follows $\lambda = 1.55\mu m$, $\varepsilon_m = -132 + 12.6i$ (gold), $\varepsilon_t = 1.0$.

Consider a single metal film with width d_0 and dielectric function ε_m embedded in a dielectric (with constant ε_t) (see Fig.2.2 with $d_j = 0,\ j = 1 - N$). For surface modes to exist at both the interfaces waves in all the media need to be evanescent. We thus rewrite the $z-$components of the wave vectors as

$$k_{0z} \;=\; i\sqrt{k_x^2 - k_0^2\varepsilon_m} = i\bar{k}_{0z}, \quad k_{tz} = i\sqrt{k_x^2 - k_0^2\varepsilon_t} = i\bar{k}_{tz}. \tag{2.20}$$

Substituting Eqs.(2.20) in Eqs.(2.13) and (2.15) and recalling the structure of the characteristic matrix (2.5), one can rewrite the dispersion equations for the symmetric and the antisymmetric modes, respectively,

$$\varepsilon_m k_{tz} + \varepsilon_t k_{0z} \tanh(x) \;=\; 0, \tag{2.21}$$

$$\varepsilon_m k_{tz} + \varepsilon_t k_{0z} \coth(x) \;=\; 0, \tag{2.22}$$

where $x = \frac{\bar{k}_{0z}d_0}{2} = \frac{k_{0z}d_0}{2i}$. It is easy to see that Eqs. (2.21) and (2.22) coincide with Eq.(A.20) of Raether's monograph [1].

The case of a single metal-dielectric interface can easily be recovered by taking the limit $d_0 \to \infty$ leading to identical values *tanh* and *coth* (=1) for large arguments. Both the equations then reduce to the same form as follows

$$\varepsilon_m k_{tz} + \varepsilon_t k_{0z} = 0. \tag{2.23}$$

Eq.(2.23) can easily be reduced to the standard dispersion relation for surface plasmons

$$k_x = k_0\sqrt{\frac{\varepsilon_t\varepsilon_m}{\varepsilon_t + \varepsilon_m}}. \tag{2.24}$$

We now comment on the decay characteristics of the coupled modes. As can be seen from Fig. 2.4, the antisymmetric (symmetric) modes have much smaller (larger) decay and thus can propagate a longer (shorter) distance. Therefore often the antisymmetri (symmetric) modes are referred to as long range or LR (short range or SR) modes.

2.6 Gap plasmons and avoided crossings

We now restrict our attention to a symmetric metal clad waveguide with dielectric core thickness d_0, and metal claddings with width d_1. After the solution of the dispersion equations are obtained for complex k_x, the complete spatial dependence of the mode functions (for example, for the symmetric modes) in the various regions are given by

For $z \leq d_0/2$

$$\begin{aligned} H_{0y}(x,z) &= 2A_0 \cos(k_{0z}z) e^{ik_x x}, & (2.25)\\ E_{0x}(x,z) &= 2ip_{0z}A_0 \sin(k_{0z}z) e^{ik_x x}, & (2.26)\\ E_{0z}(x,z) &= -\frac{2A_0 k_x}{k_0 \varepsilon} \cos(k_{0z}z) e^{ik_x x}, & (2.27) \end{aligned}$$

for $d_0/2 < z \leq d_0/2 + d_1$

$$\begin{aligned} H_{1y}(x,z) &= (A_{1+}e^{ik_{1z}(z-d_0/2)} + A_{1-}e^{-ik_{1z}(z-d_0/2)})e^{ik_x x}, & (2.28)\\ E_{1x}(x,z) &= p_{1z}(A_{1+}e^{ik_{1z}(z-d_0/2)} - A_{1-}e^{-ik_{1z}(z-d_0/2)})e^{ik_x x}, & (2.29)\\ E_{1z}(x,z) &= -\frac{k_x}{k_0\varepsilon_1}(A_{1+}e^{ik_{1z}(z-d_0/2)} + A_{1-}e^{-ik_{1z}(z-d_0/2)})e^{ik_x x}, & (2.30) \end{aligned}$$

and for $z > d_0/2 + d_1$

$$\begin{aligned} H_{ty}(x,z) &= A_t e^{ik_{tz}(z-(d_0/2+d_1))} e^{ik_x x}, & (2.31)\\ E_{tx}(x,z) &= p_{tz}A_t e^{ik_{tz}(z-(d_0/2+d_1))} e^{ik_x x}, & (2.32)\\ E_{tz}(x,z) &= -\frac{k_x}{k_0\varepsilon_t} A_t e^{ik_{tz}(z-(d_0/2+d_1))} e^{ik_x x}. & (2.33) \end{aligned}$$

The constant A_t in Eqs.(2.31)-(2.33) are evaluated using (2.14), while $A_{1\pm}$ in Eqs.(2.28)-(2.30) are given by the solution of the following martix equation

$$\begin{pmatrix} A_{1+} \\ A_{1-} \end{pmatrix} = \begin{pmatrix} e^{ik_{1z}d_1} & e^{-ik_{1z}d_1} \\ p_{1z}e^{ik_{1z}d_1} & -p_{1z}e^{-ik_{1z}d_1} \end{pmatrix}^{-1} \begin{pmatrix} 1 \\ p_{tz} \end{pmatrix} A_t. \quad (2.34)$$

The arbitrary constant A_0 is fixed by normalization of the modes. With the field profiles known, one can also calculate the time averaged Poynting vector giving the power flow along the guide.

In what follows, we present the results for the numerical calculations pertaining to the solutions of the dispersion equations (2.13) and (2.15), and the corresponding mode characteristics. For numerical calculation we chose the following parameters: $\lambda = 1.55\mu m$, $\varepsilon_0 = 2.085$ (silica), $\varepsilon_1 = -132 + 12.6i$ (gold) [10], $\varepsilon_t = 1.0$ (air). We varied d_0 and d_1. The results for the dispersion are presented in Fig. 2.5, where we have plotted the effective index $n_{eff} = k_x/k_0$ as functions of d_0. We presented the results for both the symmetric and antisymmetric modes as well as the plasmon and oscillating modes. For reference we have plotted the cases for (a) bare silica guide with outside

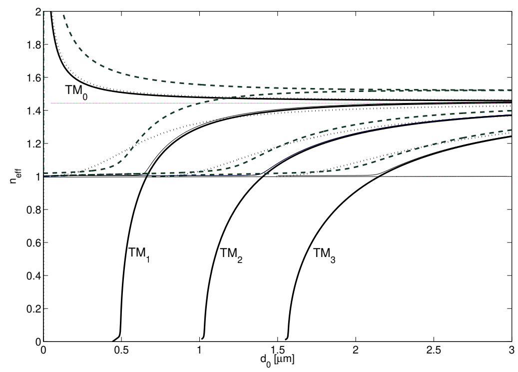

Figure 2.5: Solution of the dispersion relation for n_{eff} as functions of the core thickness d_0. The thick lines are for the semi-infinite metal claddings on the silica guide, the dotted lines are for the bare silica guide. The dashed lines are for the metal cladding thickness $d_1 = 0.01\mu m$ while the thin lines are for $d_1 = 0.03\mu m$. The parameters are as follows $\lambda = 1.55\mu m$, $\varepsilon_0 = 2.085$, $\varepsilon_1 = -132 + 12.6i$, $\varepsilon_t = 1.0$. The leaky and the higher order branches are not shown.

medium as air (dotted lines) and (b) silica guide with semi-infinite metal claddings on both sides (thick lines) [10]. A comparison of the two cases reveal clearly that with metal cladding one can realize very low effective indices (close to zero) with the oscillatory modes, while the plasmon mode offers very large values. In contrast, the guided mode indices for the silica guide are limited in the range between air and silica refractive indices (i.e., between 1 and $\sqrt{2.085} = 1.44$). In case of the GPW, one has the familiar splitting due to the coupling of the two interface plasmons. The uppermost branch (TM_0 plasmon) corresponds to the symmetric while the lower one to the antisymmetric oscillatory mode TM_1. We label the modes as plasmon (or oscillatory) depending on whether the magnetic field distribution inside the silica guide is expressible as a superposition of hyperbolic sine and cosine (or sines and cosines). Oscillatory modes from left to right are labeled by an increasing integer. It is clear from Fig. 2.5 that for semi-infinite metal claddings, there is a cut-off thickness for the oscillatory modes. For example, for $d < 0.5\mu m$, there are no oscillatory modes with the realization of a single mode operation with just the TM_0 plasmon mode. However, the scenario changes drastically if one restricts the widths of the metal cladding. For

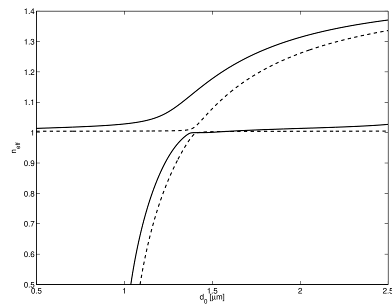

Figure 2.6: Avoided crossing phenomenon with the TM_2 mode. The solid (dashed) line is for $d_1 = 0.01\mu m$ ($d_1 = 0.03\mu m$). Other parameters are as in Fig.2.5

example, for $d_1 = 0.01\mu m$, the antisymmetric oscillatory mode exists which has a lower cut-off (see the dashed line). For a slightly larger thickness of the metal films, namely, $d_1 = 0.03\mu m$, the behavior almost coincides with the results for the guide with semi-infinite metal claddings. We have also studied the losses associated with the modes (not shown). Mode cut-off is determined by the sudden changes in the losses from small to large values as one reduces the gap width d_0. One also has the avoided crossing phenomenon like in coupled cavity-exciton systems. This results, when the metal cladding thickness is very small, leading to the possibility of coupling of the surface plasmons on the two sides of the thin cladding layer. In other words, the surface plasmon on the metal/air interface can interact with the same on the other metal/silica interface. From a somewhat different angle, this phenomenon can be viewed as the crossing of the dispersion branches of a air/silica/air guide with that of the metal/silica/metal guide. The resulting level repulsion for finite width metal cladding is shown in Fig.2.6. Indeed, the limiting cases are the bare silica guide and the gap plasmon guide with semiinfinite metal claddings. The case with finite and very low thickness of the metal cladding is in between and has the avoided crossing features. As expected, the avoided crossing effect is stronger for the lower thickness of the metal cladding. Note also that the value of the effective refractive indices for the modes corresponding to the part of the lower branches in Fig. 2.6 are less than unity. Thus these modes are leaky.

Chapter 3

More on Surface Plasmons and Coupled Surface Plasmons

3.1 Excitation Schemes for Overcoming Momentum Mismatch

Bound modes like the surface and the guided modes localized in the film or the interface are characterized by an effective index ($=k_x/k_0$) larger than the refractive index of the medium of incidence. Thus such modes can not be excited just by shining a laser beam on the film or the interface even for grazing incidence. For plane wave incidence at an angle θ_i one can never satisfy $k_0 \sin(\theta_i) = k_x = k_{g/sp}$. In order to excite them one has to compensate for the momentum mismatch. The mismatch can be overcome by a high index prism in attenuated total reflection (ATR) geometry or by periodic engravings on the surface. Such schemes are now widely used and are referred to as the prism and the grating coupling, respectively. Note that a rough surface can also couple the incident light to the relevant mode.

3.1.1 Prism Coupling: Otto, Kretschmann and Sarid Geometries

In ATR geometry one loads the guiding film or the metal-dielectric interface with a high index prism with dielectric constant ε_p, after a spacer layer, and operates at angles larger than the critical angle. Thus the waves in the spacer

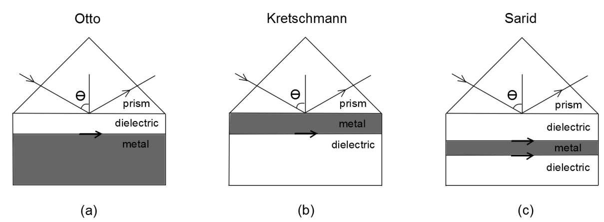

Figure 3.1: Otto, Kretschmann and Sarid geometries for ATR.

layer are evanescent and one can satisfy the momentum matching as follows

$$k_0\sqrt{\varepsilon_p}\sin(\theta_i) = k_{g,sp}. \tag{3.1}$$

In absence of the excitation of any modes, the reflectivity would be unity due to total internal reflection. For specific angles of incidence corresponding to Eq.(3.1) the modes can be excited leaving sharp dips in reflection. This signifies the channeling of the energy from the incident wave to the specified mode resulting in a corresponding drop in the reflected light. There can be variations of the ATR geometry (Fig. 3.1). The Otto geometry [11] has a low index spacer layer between the high index prism and the metal film, whereas, in the Kretschmann configuration [12] the metal film is deposited on the base of the high index prism. A different geometry, which can support coupled surface plasmons in very thin metal films, was suggested by Sarid [13]. In the Sarid geometry one can excite both the symmetrical short-range (SR) and the antisymmetrical long-range (LR) surface plasmons.

3.1.2 Grating Coupling: Analogy to Quasi Phase Matching

In this scheme the incident light falls on a grating with grating vector K ($= 2\pi/\Lambda$, Λ grating period). The period can be chosen such that one of the diffraction orders, namely, the m-th order matches the guided/surface mode

$$k_{g/sp} = k_0\sin(\theta) + mK, \quad m = \pm1, \pm2, \ldots \tag{3.2}$$

Momentum matching with the $+1$ diffraction order is shown in Fig. **??**. The dips for the coupled plasmon modes of a free standing metal film (see Fig. **??**) are shown in Fig. 3.3 [14, 15]. The results for the specular intensity

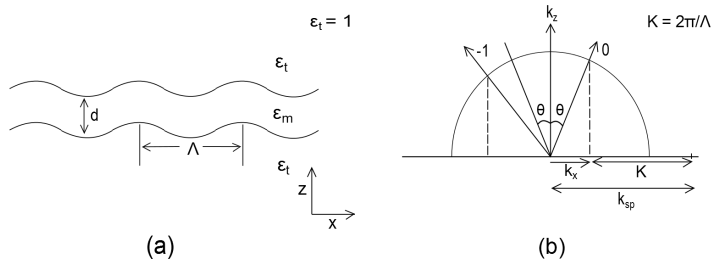

Figure 3.2: Schematics of grating coupling.

??

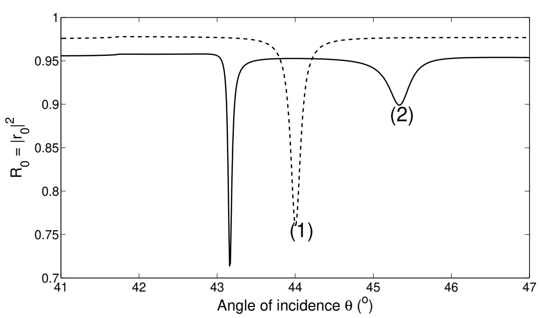

Figure 3.3: Reflected intensity as a function of angle of incidence for a silver corrugated film. The parameters are $\lambda = 633$ nm, $\varepsilon_m = -18.0 + 0.51i$, $\varepsilon_t = 1.0$, $d = 150$ nm in (1) and $d = 50$ nm in (2), $a = 8$ nm and $\Lambda = 1.893\mu m$.

reflection for a silver film of corrugation amplitude a are shown in Fig. 3.3 which clearly shows the splitting for lower film thickness.

There is an interesting example where such grating assisted momentum compensation is employed in nonlinear optics. For example, for efficient second harmonic generation the momentum mismatch Δk defined as $\Delta k = 2k_\omega - k_{2\omega}$ is compensated by the m-th order of the domain reversal grating

$$\Delta k = mK, \tag{3.3}$$

and for a first order process domain reversal period is chosen as $\Lambda = 2\pi/\Delta k$ which is just double of the coherence length beyond which synchronised propagation of fundamental and second harmonic is not possible.

3.2 Local field Enhancements: Applications

A close inspection of the expressions of the reflection and transmission amplitudes (2.7) and a mere appreciation of the fact that modes correspond to poles of these coefficients (see Eq.(2.8)), immediately leads to the understanding of the remarkable potentials of these modes. 'Diverging' r and t implies dramatic enhancements of the local fields which opens up a host of applications. The narrower the mode resonance (lower decay), the tighter it is bound to the surface and the larger is the enhancement. In the context of Kretschmann geometry, large transmitted amplitude does not violate any energy conservation, since the transmitted wave is evanescent and it does not carry any energy.

The long-range surface plasmons (LRSP) have the added advantage of large local field enhancements associated with them (Sarid, Deck, Craig, Hickernell, Jameson and Fasano [16, 17]. Various nonlinear optical phenomena exploiting narrow LRSP modes were demonstrated by Sarid's group and others [18, 19, 20]. Optical bistability with surface plasmons at a metal-nonlinear dielectric interface was demonstrated by many (see references in [5]). We investigated optical bistability in the prism-metal film-nonlinear substrate configuration without the assumption of a plane wave solution for the nonlinear dielectric [21]. Exact results for optical bistability with surface plasmons in a layered structure on a nonlinear substrate were presented by us [22] using the solutions of Leung [23].

There have been other notable applications of the local field enhancement effect in surface enhanced Raman processes, in high resolution spectroscopy, single molecule spectroscopy and many other areas. As mentioned before detailed description of all such applications is much beyond the scope of these notes.

Chapter 4

Related Interesting Physics

In this chapter we report on some interesting fundamental effects which could be explored for plasmonic systems to lead to yet exciting novel applications. I will just cite one example: phase sensitive measurements via the Goos-Hänchen shift have recently led to order of magnitude enhancement in the resolution of a SPP sensor [24].

4.1 An Interesting Parallel

We first look at a parallel between seemingly different phenomena. The first one is in the time domain when one poses a question on the time taken by a localized pulse (like a Gaussian pulse) in passing through a sequence of barriers and wells. Equivalent question in optics will address the propagation of a pulse through a stratified medium. The second one refers to a finite in space beam, say, a Gaussian fundamental beam being reflected at an interface between two dielectrics. The former leads to the Wigner delay [25], while the latter gives a longitudinal shift known as the Goos-Hänchen shift [26]. Both the effects are due to the age-old finite vs infinite issue. In the following we study them using the same stationary phase approximation and arrive at analogous expressions.

4.1.1 Wigner Delay

In this subsection, we generalize the derivation of Wigner [25] with bichromatic light to the case of a temporal pulse centered around the carrier frequency ω_c. Let the incident pulse be given by

$$E_I(z,t) = F(t)e^{i(\beta z - \omega_c t)}, \tag{4.1}$$

where the Fourier decomposition of the temporal profile at $z = 0$ is written as

$$F(t) = \int A(\omega)e^{-i(\omega-\omega_c)t}d\omega. \tag{4.2}$$

Let $\tilde{t}(\omega)$ be the complex transmission coefficient of the medium given in terms of the real amplitude and phase as follows

$$\tilde{t}(\omega) = |\tilde{t}(\omega)|e^{i\phi_T(\omega)}. \tag{4.3}$$

Using Eqs.(4.1) - (4.3), the transmitted pulse (in the region $z > L$) can be written as

$$E_T(z,t) = e^{i(\beta z - \omega_c t)} \int A(\omega)|\tilde{t}(\omega)|e^{i\phi_T(\omega)}e^{-i(\omega-\omega_c)t}d\omega. \tag{4.4}$$

The temporal shift of the transmitted pulse, depends on ϕ_T which bears the signature of the dispersion of the medium. In order to estimate the temporal shift of the pulse we expand ϕ_T in Taylor series around ω_c

$$\phi_T(\omega) = \phi_T(\omega_c) + \left.\frac{\partial\phi_T}{\partial\omega}\right|_{\omega_c}(\omega - \omega_c) + \cdots\cdots. \tag{4.5}$$

On substituting the above expansion in Eq.(4.4) and retaining only terms up to the first order we get

$$E_T(z,t) = e^{i(\beta z - \omega_c t + \phi_T(\omega_c))} \int A(\omega)|\tilde{t}(\omega)|e^{-i\left(t - \left.\frac{\partial\phi_T}{\partial\omega}\right|_{\omega_c}\right)(\omega-\omega_c)}d\omega. \tag{4.6}$$

Assuming a flat (or slowly varying) amplitude response ($|\tilde{t}(\omega)| \sim$ constant) over the spectral spread of $A(\omega)$, Eq.(1.19) reduces to the following

$$E_T(z,t) = |\tilde{t}(\omega_c)|F\left(t - \left.\frac{\partial\phi_T}{\partial\omega}\right|_{\omega_c}\right)e^{i(\beta z - \omega_c t + \phi_T(\omega_c))}. \tag{4.7}$$

Thus the transmitted pulse arrives at the output end (i.e. $z = L$) at

$$\tau_T = \left.\frac{\partial\phi_T}{\partial\omega}\right|_{\omega_c}. \tag{4.8}$$

Similarly, the reflected pulse will be delayed/advanced by

$$\tau_R = \left.\frac{\partial \phi_R}{\partial \omega}\right|_{\omega_c}, \tag{4.9}$$

where ϕ_R is the phase of the reflection coefficient.

A representative calculation for the gap plasmon guide of section 2.6 is shown in Fig. 4.1. We have plotted the intensity reflection coefficient T and the Wigner delay τ as functions of angle of incidence θ

4.1.2 Goos-Hänchen Shift

The derivation for the Goos-Hanchen shift is quite analogous, except that the incident field is now assumed to be a monochromatic beam with a spread of wave vector around (α_0, β), where α and β are the x and z components of the wave vector. The interface between the two dielectrics is assumed to be the plane $z = 0$. Thus the incident field can be written as

$$E_I(x,t) = e^{i(\alpha_0 x + \beta z - \omega_0 t)} \int A(\alpha) e^{i(\alpha - \alpha_0)x} d\alpha. \tag{4.10}$$

As mentioned above, the divergence of the Fourier components are so small that $A(\alpha)$ is sharply peaked around α_0 with the corresponding angle of incidence $\theta_0 >$ critical angle θ_c. Thus, the total internal reflection condition is assumed to be valid for all Fourier components and the reflected pulse can then be written as

$$E_R(x,t) = e^{i(\alpha_0 x - \beta z - \omega t)} \int A\left(\alpha\right) e^{i(\alpha - \alpha_0)x + i\phi_R(\alpha)} d\alpha, \tag{4.11}$$

where $\phi_R(\alpha)$ is the phase of the complex reflection coefficient. An expansion of $\phi_R(\alpha)$ around α_0 just like in Eq.(4.5) reduces Eq.(4.11) to

$$E_R(x,t) = e^{i(\alpha_0 x - \beta z - \omega t + \phi_R(\alpha_0))} \int A\left(\alpha\right) e^{i(\alpha-\alpha_0)\left(x + \left.\frac{\partial \phi_R}{\partial \alpha}\right|_{\alpha_0}\right)} d\alpha. \tag{4.12}$$

With a definition of the incident beam profile at $z = 0$ as

$$F(x) = \int A(\alpha) e^{i(\alpha - \alpha_0)x} d\alpha, \tag{4.13}$$

the reflected beam takes the final form given by

$$E_R = F\left(x + \left.\frac{\partial \phi_R}{\partial \alpha}\right|_{\alpha_0}\right) e^{i(\alpha_0 x - \beta z - \omega t) + i\phi_R(\alpha_0)}, \tag{4.14}$$

which implies a longitudinal displacement of the beam by an amount

$$d = -\left.\frac{\partial \phi_R}{\partial \alpha}\right|_{\alpha_{0.}}. \tag{4.15}$$

4.1.3 Resonant Tunneling and Slow Light, Critical Coupling and Coherent Perfect Absorption

Here we give a brief overview of some of the widely studied structures of interest in the context of the surface/guided excitations.

Resonant tunneling and slow light

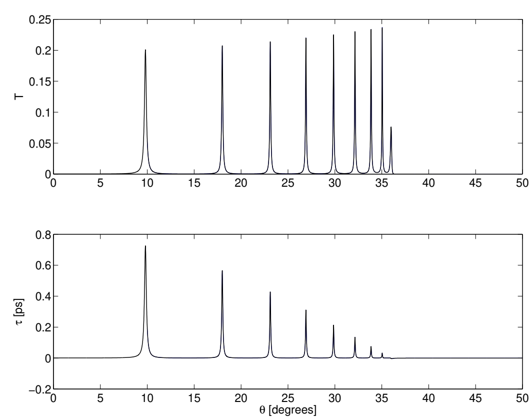

Figure 4.1: (a) Intensity transmission coefficient T and the (b) Wigner delay τ as functions of the angle of incidence θ for $d_0 = 3.0\mu m$, $d_1 = 0.03\mu m$, $\varepsilon_t = 6.145$. The other parameters are as in Fig.2.5

A typical example of a resonant tunneling structure is the GP guide (discussed in section 2.6) enclosed between two high index prisms, where waves are evanescent in the metal layers. It can be evanescent or propagating in the central dielectric layer depending on which modes are excited. For plane wave incidence at an arbitrary angle, very little will be transmitted. There can be significant transmission only via the resonant states. This is referred to as resonant tunneling. One such case is shown in the top plot of Fig. 4.1 for a multimode GP guide. Different peaks correspond to the different modes. In order to determine the delay characteristics of the structure, we extract the phase of the transmission coefficient. The frequency derivative of the phase of amplitude transmission (see Eq.(4.8)) then gives the Wigner delay through the structure [25]. Fig. 4.1 clearly shows how light is slowed down when these modes are excited.

Critical coupling

A system is said to be critically coupled (CC) to incident radiation, when there is no scattering from it resulting in total absorption of the incident energy. In the context of a stratified medium this would mean simultaneously null transmission as well as null reflection. Such a situation can arise as a delicate balance when all the reflected (transmitted) components from all interfaces result in complete destructive interference. Such systems exploiting the metal-dielectric nano composites have been proposed [27] and analogous systems have been realized in experiment. In the context of CC leading to complete absorption, one needs to consider the energy conservation condition given by $R+T+A=1$ (A - absorption of the structure). Since most of the incident energy goes in absorption, the total scattering ($R+T$) of a critically coupled system must be near zero.

Coherent Perfect Absorption (CPA)

Past couple of years have seen a great deal of interest in CPA or anti-lasing, which is a generalisation of the CC concept to multiple incident beams [28, 29]. Again the underlying mechanism is the complete destructive interference and a CPA device can be understood as a time reversed analogue of a laser near threshold. [29]

4.1.4 Nonreciprocity

Optical theorem can have interesting consequences in the context of stratified media and broken spatio-temporal symmetry [30, 31]. Nonidentical reflection under illumination from opposite sides was monitored in a system of two lossless coupled cavities, when the spatio-temporal symmetry was broken by introducing lossy resonant quantum wells in one of the cavities. Recently such nonreciprocity was shown to lead to GH shifts with opposite signs, which can lead to extra-sensitive displacement monitors with resolution of few nano meters [32].

Acknowledgement

I would like to thank Rahul for his help in preparing some of the codes, figures and the manuscript. I am also thankful to all the participants for their attention and patience.

Bibliography

[1] H. Raether, *Surface Plasmons on Smooth and Rough Gratings*, (Springer, Berlin, 1988).

[2] H. Raether, in *Physics of Thin-Films* (Academic, New York, 1977), Vol. 9, pp. 145-261.

[3] S. A. Maier, *Plasmonics: Fundamentals and Applications*, (Springer, NY, 2007).

[4] M. Born and E. Wolf, *Principles of Optics* (Pergamon, New York,1980), Chap. 1.6.

[5] S. Dutta Gupta, 'Nonlinear optics of stratified media' in *Progress in Optics* vol 38, ed. E. Wolf (Elsevier, Amsterdam, 1998) pp 1-84.

[6] S. Dutta Gupta, *Pramana - J Phys.* **72**, 303 (2009).

[7] There are three major sources of data for the dielectric function of the noble metals: the Drude model, Johnson and Christie data and the data in E D Palik's handbook. These data sources do not match and there is some debate on which is the best. A detailed comparison was made by Atwater's group but they also do not pass a final verdict on this issue. See for example, J. A. Dionne, L. A. Sweatlock, H. A. Atwater and A. Polman, *Phys. Rev. B* **72**, 075405-1, (2005); J. A. Dionne, L. A. Sweatlock, H. A. Atwater and A. Polman, *Phys. Rev. B* **73**, 035407-1, (2006). We rely on the Johnson and Christie data [8].

[8] P. B. Johnson and R. W. Christy, 'Optical Constants of the noble metals', *Phys. Rev. B* **6**, 4370-4379 (1972).

[9] S. Dutta Gupta and G. S. Agarwal, *Opt. Comm.* **103**, 122 (1993).

[10] Pavel Ginzburg, David Arbel and Meir Orenstein, *Opt. Lett.* **31**, 3288-3290 (2006).

[11] A. Otto, 'Excitation of nonradiative surface plasma waves in silver by the method of frustrated total reflection', *Z. Phys.* **216**, 398-410 (1968).

[12] E. Kretschmann, *Z. Phys.* **241**, 313 (1971).

[13] D. Sarid, 'Long-Range Surface-Plasma Waves on Very Thin Metal Films', *Phys. Rev. Lett.* **47**, 1927 (1981).

[14] T. Inagaki, M. Motosuga, E. T. Arakawa and J. P. Goudonnet, 'Coupled surface plasmons in periodically arranged thin silver films', *Phys. Rev. B* **32**, 6238 (1985).

[15] S. Dutta Gupta, G. V. Varada and G. S. Agarwal, 'Surface plasmons in two-sided corrugated thin films' *Phys. Rev. B* **36**, 6331 (1987).

[16] D. Sarid ,R.T. Deck A.E. Craig, R.K. Hickernell, R.S. Jameson and J.J. Fasano *Appl. Opt.* **21**, 3993 (1982).

[17] G. S. Agarwal *Phys. Rev. B* **31**, 3534 (1985).

[18] D. Sarid ,R. T. Deck and J. J. Fasano *J. Opt. Soc. Am. B* **72**, 1345 (1982).

[19] R. T. Deck and D. Sarid *J.Opt. Soc. Am.* **72**, 1613 (1982).

[20] J. C. Quail, J. G. Rako, H.J. Simon and R.T. Deck, *Phys. Rev. Lett.* **50**, 1987 (1983).

[21] S. Dutta Gupta, G. S. Agarwal, *J. Opt. Soc. Am. B* **3**, 236 (1986).

[22] G. S. Agarwal and S. Dutta Gupta *Phys. Rev. B* **34**, 5239 (1986).

[23] K. M. Leung *Phys. Rev. A* **33**, 2461 (1986).

[24] X. Yin, L. Hesselink, *Applied Physics Letters* **89**, 261108 (2006).

[25] E. P. Wigner, *Phys. Rev.*, **98**, p.145 (1955).

[26] F. Goos, H. Hänchen, *Annalen der Physik (Leipzig)* **1**, 333 (1947).

[27] S. Dutta Gupta,'Strong interaction mediated critical coupling at two distinct frequencies' *Opt. Lett.* **32**, 1483-1485 (2007).

[28] Wenjie Wan, Yidong Chong, Li Ge, Heeso Noh, A. Douglas Stone and Hui Cao, 'Time-Reversed Lasing and Interferometric Control of Absorption' *Science* **331**, 889 (2011).

[29] Shourya Dutta Gupta, O. J. F. Martin, S. Dutta Gupta and G. S. Agarwal, 'Controllable coherent perfect absorption in a composite film' *Opt. Express* **20**, 1330-1336 (2012).

[30] A. Armitage, M. S. Skolnik, A. V. Kavokin, D. M. Whittaker, V. N. Astratov, G. A. Gehring, and J. S. Roberts, *Phys. Rev. B* **58**, 15,376 (1998).

[31] G. S. Agarwal and S. Dutta Gupta, 'Reciprocity relations for reflected amplitudes' *Opt. Lett.* **27**, 1205 (2002).

[32] Madhuri Kumari, S. Dutta Gupta, 'Positive and negative giant Goos-Hänchen shift in a near-symmetric layered medium for illumination from opposite ends', *Opt. Comm.* **285**, 617 (2012).

Appendix

Matlab Code for the Solution of the Coupled Plasmon Dispersion

Function to be minimized and the main code for the symmetric branch

```
function f1=spfun(nd);
global d lam epst epsm;
nx=nd(1)+i*nd(2);
k0=2*pi/lam;

nxt=sqrt(epst-nx^2);
if imag(nxt)<0;
    nxt=-nxt;
end

nxm=sqrt(epsm-nx^2);
if imag(nxm)<0;
    nxm=-nxm;
end
b1=k0*d*nxm/(2*i);
bth=tanh(b1);
rd=nxm*epst+nxt*epsm*bth;
f1(1)=real(rd);
f1(2)=imag(rd);
******************
%symmetric plasmon.m
```

```
clear all; clc;
global d lam epst epsm;
% system parameters
 lam=1.55; epst=1;
 epsm=-132+12.6*i;

di=0.001; df=0.1; nn=500;  dt=(df-di)/nn;
nef0=[2 -0.1];dd=[]; ner=[]; nim=[];
for k=1:nn+1;
    d=di+(k-1)*dt;
    %options=optimset('Display','notify');
    [effn,fval,exitflag]=fsolve(@spfun,nef0);
    if exitflag<=1;exitflag
    dd=[dd d];
    ner=[ner effn(1)];
    nim=[nim effn(2)];
    nef0=effn;
    end
end
plot(dd,ner,'.');hold on;
%plot(dd, sqrt(epst),'-.')
```

Function to be minimized and the main code for the antisymmetric branch

```
function f1=spfun(nd);
global d lam epst epsm;
nx=nd(1)+i*nd(2);
k0=2*pi/lam;

nxt=sqrt(epst-nx^2);
if imag(nxt)<0;
    nxt=-nxt;
end

nxm=sqrt(epsm-nx^2);
if imag(nxm)<0;
```

```
    nxm=-nxm;
end
b1=k0*d*nxm/(2*i);
bth=coth(b1);
rd=nxm*epst+nxt*epsm*bth;
f1(1)=real(rd);
f1(2)=imag(rd);
****************
%antisymmetric plasmon.m
clear all; clc;
global d lam epst epsm;
% system parameters
 lam=1.55; epst=1;
 epsm=-132+12.6*i;

di=0.1; df=0.001; nn=500;  dt=(df-di)/nn;
nef0=[1 0.001];dd=[]; ner=[]; nim=[];
for k=1:nn+1;
    d=di+(k-1)*dt;
    %options=optimset('Display','notify');
    [effn,fval,exitflag]=fsolve(@antispfun,nef0);
    if exitflag<=1;exitflag
    dd=[dd d];
    ner=[ner effn(1)];
    nim=[nim effn(2)];
    nef0=effn;
    end
end
plot(dd,ner,'.');hold on;
%plot(dd, sqrt(epst),'-.')
```